ISSN 2075-1133, Inorganic Materials: Applied Research, 2025, Vol. 16, No. 3, pp. 914–924. © Pleiades Publishing, Ltd., 2025.
Russian Text © The Author(s), 2024, published in Fizika i Khimiya Obrabotki Materialov, 2024, No. 6, pp. 52–66.

NEW METHODS OF TREATMENT AND PRODUCTION OF MATERIALS WITH REQUIRED PROPERTIES

Effect of Creep on the Microstructure of Aluminum Alloy AD1 in Recrystallized and Ultrafine-Grained States

S. S. Manokhin[a, *], D. A. Kolesnikov[b], I. V. Nelasov[a], Yu. R. Kolobov[a, **], D. V. Lazarev[b], V. I. Betekhtin[c], A. G. Kadomtsev[c], and M. V. Narykova[c]

[a] *Federal Research Center for Problems of Chemical Physics and Medical Chemistry, Russian Academy of Sciences, Chernogolovka, 142432 Russia*

[b] *Belgorod State National Research University (BelSU), Belgorod, 308015 Russia*

[c] *Ioffe Physical-Technical Institute, Russian Academy of Sciences, St. Petersburg 194021 Russia*

**e-mail: manohin@icp.ac.ru*

***e-mail: kolobov@icp.ac.ru*

Received December 5, 2023; revised December 22, 2023; accepted August 5, 2024

Abstract—The changes in the microstructure of industrial aluminum alloy AD1 in recrystallized and ultrafine-grained (UFG) states are studied before and after creep tensile tests at $0.3T_{melt}$ (100°C). It is established that, in the recrystallized structure, creep leads to the fragmentation of large elongated grains into smaller grains and subgrains, accompanied by an increase in the fraction of low-angle boundaries. In the UFG structure, grain growth (collecting recrystallization) is observed during the creep. A strong radial texture is identified, where the crystalline lattices of the alloy grains are predominantly oriented along the [001] crystallographic direction parallel to the axis of the original round rod (parallel to the rolling direction). This texture is typical of both recrystallized and ultrafine-grained samples. After creep tests, the UFG samples exhibit a shift in direction of the texture axis from [001] to [011]. This is accompanied by formation of particles of the secondary phase—aluminum carbide and silicon compounds—which is confirmed through CALPHAD phase diagram calculations. The dislocation structure of aluminum alloy AD1 is explored.

Keywords: aluminum alloy, recrystallization, ultrafine-grained material, structure, phase, low-temperature creep, scanning electron microscopy, transmission electron microscopy, texture, microstructure, average grain size

DOI: 10.1134/S2075113325700832

INTRODUCTION

A fundamental challenge in strength physics deals with evaluating the operational life span (durability) of structural materials and developing methods to enhance it. It is known that, during the entire period of material loading, plastic loosening (decompaction) is accumulated, primarily due to generation of defects such as pores and cracks [1–3]. Pore and crack formation begins almost immediately upon loading at the early stages of plastic deformation. Nanopores were shown to nucleate already at the stage of forming submicrocrystalline (SMC) or nanostructured (NS) states in metallic materials exposed to plastic deformation [4].

Identifying the parameters of the defect structure in metallic materials that facilitate the transition to the final stage of destruction, as well as the kinetic patterns to generate deformation under prolonged loading, is important from the scientific standpoint. The role of porosity is especially important in influencing the properties of solids, including behavior of fractures [5].

The contribution of defects (nanopores and nanofractures) formed by both effects of plastic deformation and subsequent tests on the long-term strength of UFG materials are not sufficiently covered in the domestic and foreign literature.

Let us clarify some issues related to the terminology. In the last two decades, ultrafine-grained (UFG) (grain size of 1–10 μm), sub-microcrystalline (SMC) (grain size of 0.1–1 μm), and nanostructured (NS) (grain size on the order of 0.1 μm or smaller) metals and alloys obtained by plastic [6–9] as well as megaplastic (MPD) deformation have been intensively researched and increasingly used in medicine and engineering [10]. In all cases, the deformation process developed under high applied pressures, resulting in dramatic plastic deformation. In contrast to above classification of the grain structure of materials, the term ultrafine-grained materials, referring to materials produced by severe plastic deformation and having an average microstructure size of less than 1 μm, was widely used in the English and partly domestic litera-

ture in the last decade. At the same time, the traditional term ultrafine grain in metals, known to domestic and foreign authors by the monograph having the same title [11], was replaced without discussion among experts. As noted above, the term applies to the structure having a grain size of 1–10 μm. The reason for the special designation of this size interval dealt with the fact that, at the time the term became popular, alloys having this structure revealed the effect of structural superplasticity. We follow the terminology described in [8] and well established in the domestic literature, according to which polycrystals have a grain size in the interval of 1–10 μm.

Thus, a comparative study of the microstructure of the recrystallized and ultrafine-grained materials that we examine after durability tests is important from a scientific and practical point of view.

The aim of the work was to study the influence of the creep process on changes in the structure of recrystallized and ultrafine-grained aluminum alloy by modern analytical methods.

MATERIALS AND METHODS

The elemental composition of AD1 aluminum (according to GOST 4784-97) is given in Table 1.

Previously, we developed mechanical and heat treatment regime for alloys of technically pure titanium and various grades of aluminum using longitudinal and helical rolling, which make it possible to obtain bars of SMC and NS titanium and SMC and UFG aluminum with diameter of 4–10 mm [8]. In this work, we used AD1 aluminum alloy bars (OD 8 mm) in the original SMC state. The bars were previously exposed to recrystallized annealing at 250°C for 1 h. After annealing, the alloy featured a uniform grain-subgrain structure (UFG state), the arithmetic mean size of structural elements being on the order of 1.5 μm.

Recrystallized and UFG samples of AD1 aluminum alloy were supplied by the customer and we carried out research using them. The conditions to run the tests are listed in Table 2.

The microstructure of the samples was studied by transmission electron microscopy (TEM) using an FEI Tecnai Osiris microscope having an acceleration voltage of 200 kV (including the scanning electron microscopy mode). The TSL OIM Data Collection and TSL OIM Analysis, version 6.21 (EDAX) packages were used to compile the map of grain orientations and pole shapes and for data processing, respectively.

Preparation of thin foils (lamellae) cut perpendicularly to the surface of the sample from the area of break of the sample after creep tests for transmission electron microscopy was carried out by the focused ion beam ion thinning method in the column of a FEI Scios focused ion beam scanning electron microscope (at the Federal Scientific Research Center Crystallography and Photonics), with the potential of carrying out electron backscatter diffraction (EBSD) analysis for an acceleration voltage of 20 kV and for the sample surface oriented at 70° to the direction of the electron beam [12]. No additional defects can be generated in the sample when this surface treatment method is used. The lamellae were cut in the fracture area some 1.6 mm away from the fracture at a depth of 250 μm from the surface (Fig. 1).

When thin foil was made using an electrolytic method, we followed the standard technique; namely, we applied a platinum-based protective coating. This was required to obtain a smooth cross section keeping thin layers underpinning the surface layer intact. An ion beam was used to cut an area up to 10 μm wide along the working plane of the initial cut and up to 8 μm deep next to the sputtered platinum strip. Ion thinning of the modified surface (perpendicular to the surface) resulted in obtaining thin samples of aluminum approximately 70 nm thick with a region of interest of approximately 10×8 μm^2 for subsequent TEM studies.

Table 1. Chemical composition of aluminum alloy grade AD1. GOST 4784-97

Alloy grade AD1	Content of elements, wt %. Base—Al							
	Fe	Si	Ti	Zn	Cu	Mg	Mn	admixtures
Requirements	≤0.3	≤0.3	≤0.15	≤0.1	≤0.05	≤0.05	≤0.025	≤0.05

Table 2. Test parameters of samples of AD1 alloy

Sample number	Sample conditions	Temperature, T, °C	Normal strain during deformation, σ, MPa	Degree of deformation, ε, %	Time, τ, s
1	Recrystallized	100	113	12	19600
2	Submicrocrystalline			9.4	19600
3				20	36120

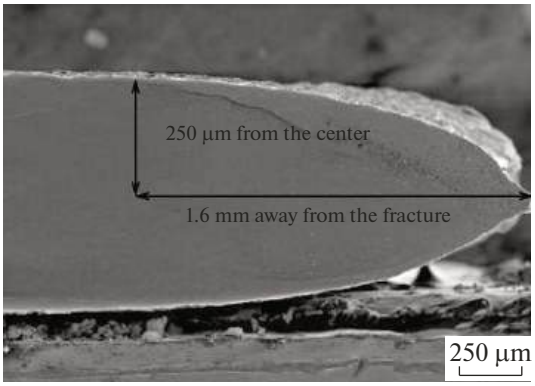

Fig. 1. Area of manufacture of sample of AD1 grade alloy.

RESULTS AND DISCUSSION

The study of recrystallized and UFG samples of the alloy was carried out in the area of the working base using EBSD analysis. Both samples had grains elongated along the axis of the bar. The size of grains was different in recrystallized and UFG samples (Fig. 2).

The average length of the grains in the structure of the recrystallized sample was about 7–9 μm, and in cross section, the length was about 2–2.5 μm. The grain non-equiaxiality coefficient in the longitudinal section of the sample was 2.3. In the cross section, the grains had a globular shape. In UFG aluminum, these dimensions were 4–5 and 1 μm, respectively (Figs. 2b, 2d), the non-equiaxiality coefficient in longitudinal was about 3.6.

The smaller degree of elongation of grains in the recrystallized state if compared to UFG indicates development of high-angle boundaries for the part of the small-angle boundaries (sub-boundaries) in grains during recrystallization annealing. In the longitudinal section, for both types of samples, the major fraction was the small angle boundaries. The share of these

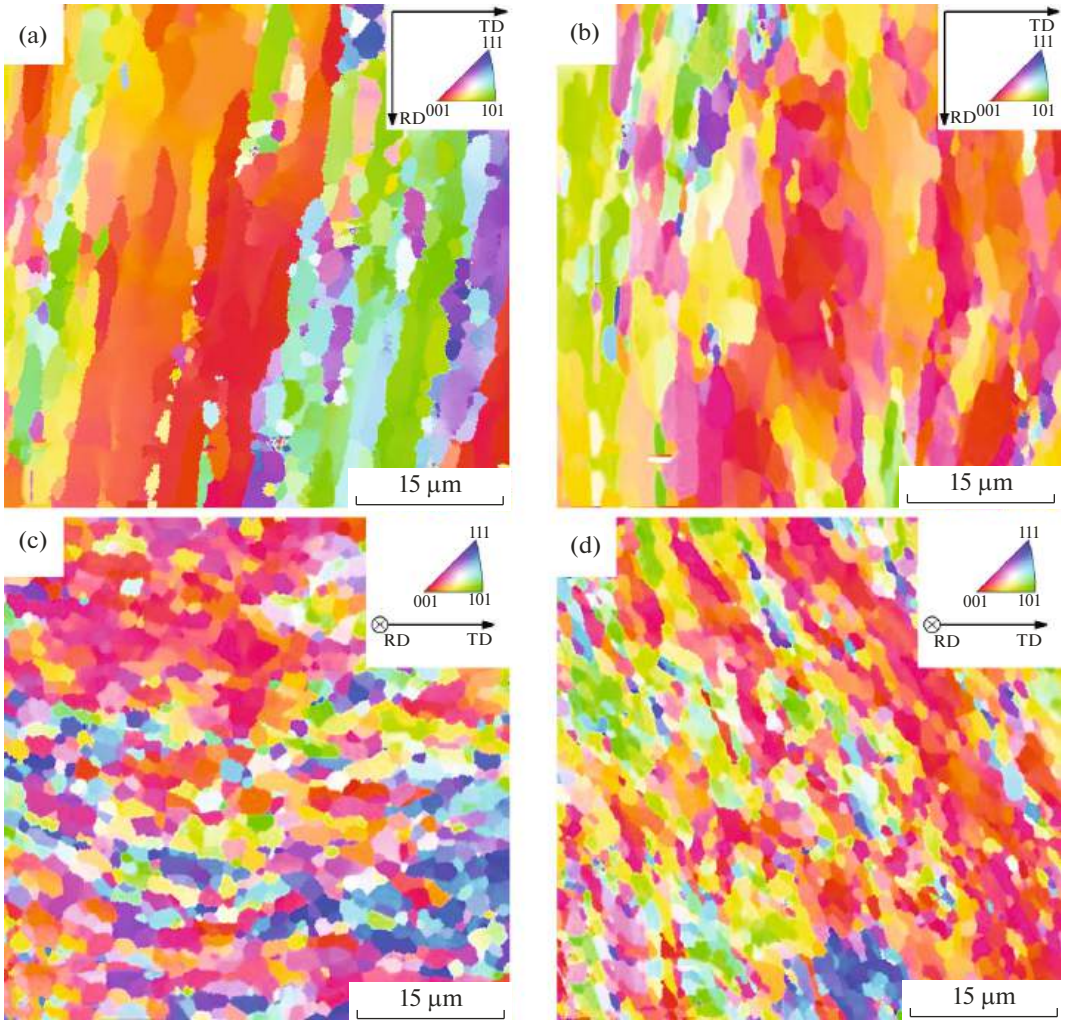

Fig. 2. Orientation maps of the grain structure of samples in the initial state (made from the area of the working base of sample) in the longitudinal (a, b) and cross (c, d) sections. (a, c) Recrystallized state; (b, d) ultrafine-grained state. Grain orientation maps are color-coded. Direction [001] is oriented along the normal to the surface of the sample.

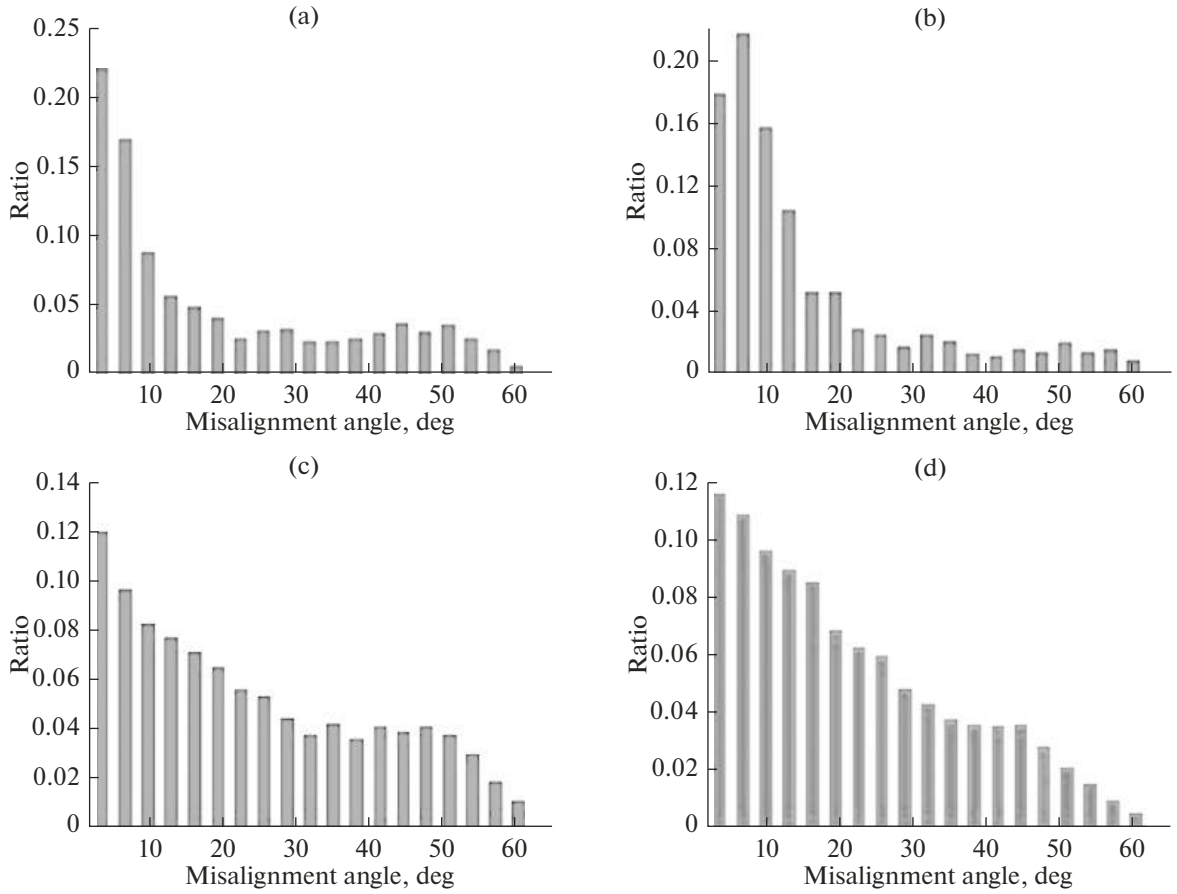

Fig. 3. Histograms of grain misalignment angles plotted for the original sample in the longitudinal (a, b) and cross (c, d) sections. (a, c) Recrystallized state; (b, d) ultrafine-grained state.

boundaries in UFG structure was above 65%, while in the recrystallized state this number dropped to 53% (Figs. 3a, 3b). The cross section of both types of structures was dominated by high-angle grain boundaries, with a higher content being observed in the recrystallized sample (Figs. 3c, 3d).

The studies on the structure of recrystallized and ultrafine-grained aluminum alloy after backscatter electron creep tests revealed that the fracture region was occupied by grains having a smaller average length in the recrystallized samples, whereas the size in the transverse direction was larger (Fig. 4).

The average grain length in recrystallized sample after tests (σ = 113 MPa, τ = 19600 s) decreased from 7–9 to 3–4 μm, and in the transverse direction, it increased from 2–2.5 to 3–4 μm. This change was accompanied by an increase in the number of small-angle boundaries from 53 to 66% and by formation of special double-type boundaries, indicating that dynamic recrystallization took place during testing. The share of special boundaries was about 3–4%, as evidenced by the peak grain-boundary angle equal to about 57° (Fig. 5a).

Samples with a reference UFG structure showed grain growth in both the longitudinal and transverse directions after the creep tests. A significant increase in the average grain size indicated an intense dynamic recrystallization. Thus, on one hand, the dynamic recrystallization that developed during the tests resulted in increasing the diameter of the grains in the transverse direction and, on the other hand, in fragmentation of the long grains through forming small-angle grains and, in some cases, the grains having special boundaries.

The texture analysis revealed the presence of a strong radial texture with the texture axis [001] pointing along the axis of the bar in both (recrystallized and UFG) reference samples. In the recrystallized sample, texturing along the axis [011] (bimodal texture character, Figs. 6a, 6c) was additionally traced. Apparently, the recrystallization annealing resulted in formation of an additional texture component (recrystallization texture).

If compared to the original sample, in the recrystallized sample after the creep tests (σ = 113 MPa, τ = 19600 s), the texture did not change; it only became more pronounced (Fig. 7).

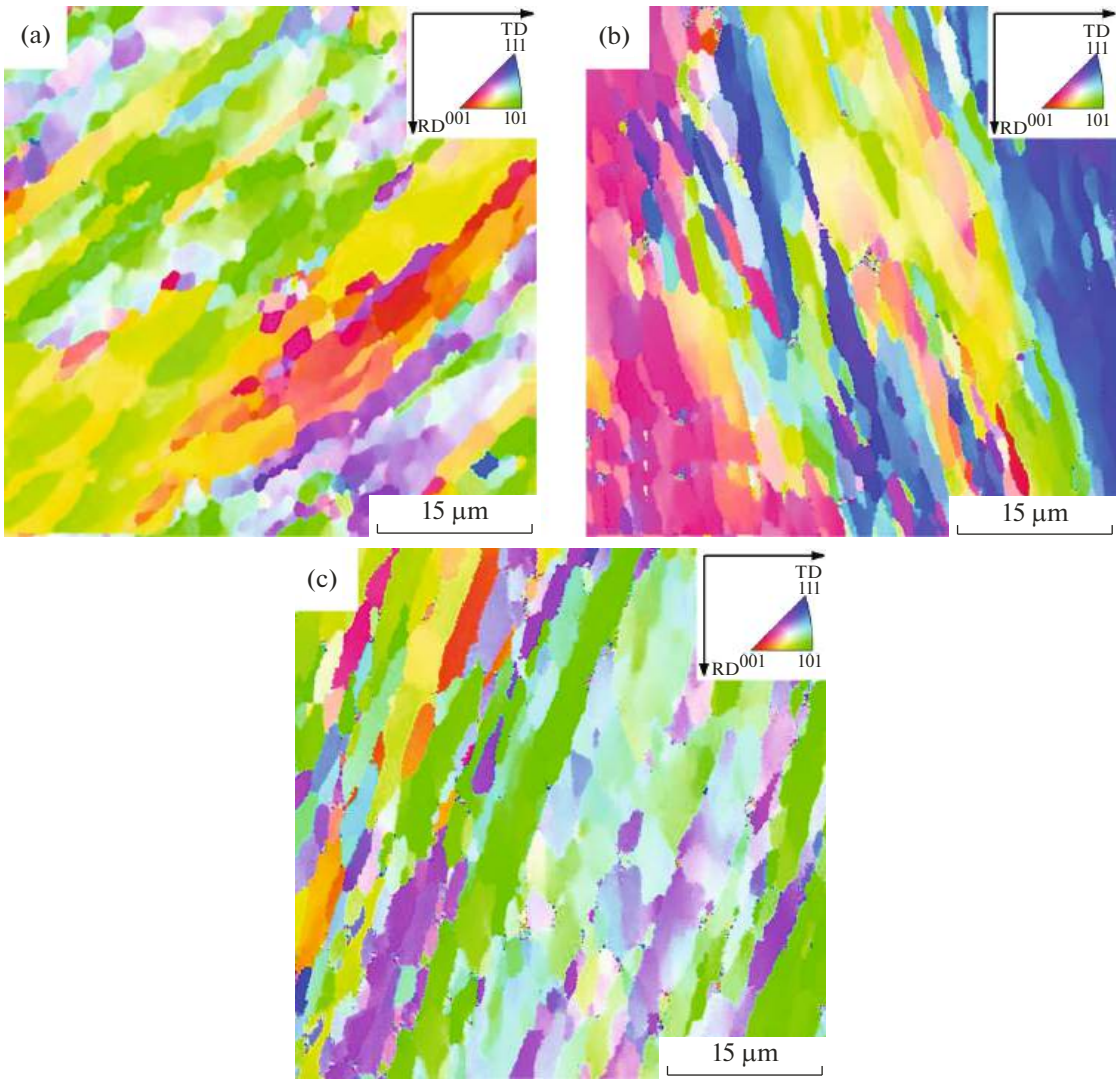

Fig. 4. Orientation maps of grain structure of samples after long-term strength tests in the fracture region in the longitudinal section: (a) recrystallized state ($\sigma = 113$ MPa, $\varepsilon = 12\%$, $\tau = 19600$ s), (b) ultrafine-grained state (rapid loading, $\sigma = 113$ MPa, $\varepsilon = 9.4\%$, $\tau = 19600$ s), (c) ultrafine-grained state ($\sigma = 113$ MPa, $\varepsilon = 20\%$, $\tau = 36120$ s). Grain orientation maps are color-coded. Direction [001] is oriented along the normal to the surface of the sample.

Following the creep tests, the samples with the reference UFG structure changed the axis of texture from [001] to [011] (Fig. 8), while the recrystallized sample had a more pronounced texture without significant changes if compared with the reference sample.

The phenomenon of texture blurring during creep was not observed in either of the samples. This suggests that the grain boundary sliding (GBS) made a minor contribution to the overall deformation, since the test temperature of 100°C is not high enough for the aluminum alloy to trigger active GBS.

The transmission electron microscopy revealed typical patterns of the microstructure in the samples of recrystallized and UFG aluminum alloy before and after long-term strength tests (Fig. 9).

The mean dislocation density in the original samples was higher for the UFG sample, the rough estimates being 10^8 cm^{-2} for the recrystallized sample and 10^9 cm^{-2} for the UFG sample.

The images of the structure obtained for recrystallized and ultrafine-grained AD1 alloy samples after long-term strength (creep) tests are shown in Fig. 10. They were obtained using an electron microscope.

After creep tests, the recrystallized sample showed an increase in the average density of dislocations to about 10^9 cm^{-2}. When the ultrafine-grained sample was quickly loaded during the creep test, the average density of dislocations was about 10^{11} cm^{-2}. When the creep test was finished and the average density of dislocations was measured after 10 h, it dropped by an order of magnitude to 10^{10} cm^{-2}.

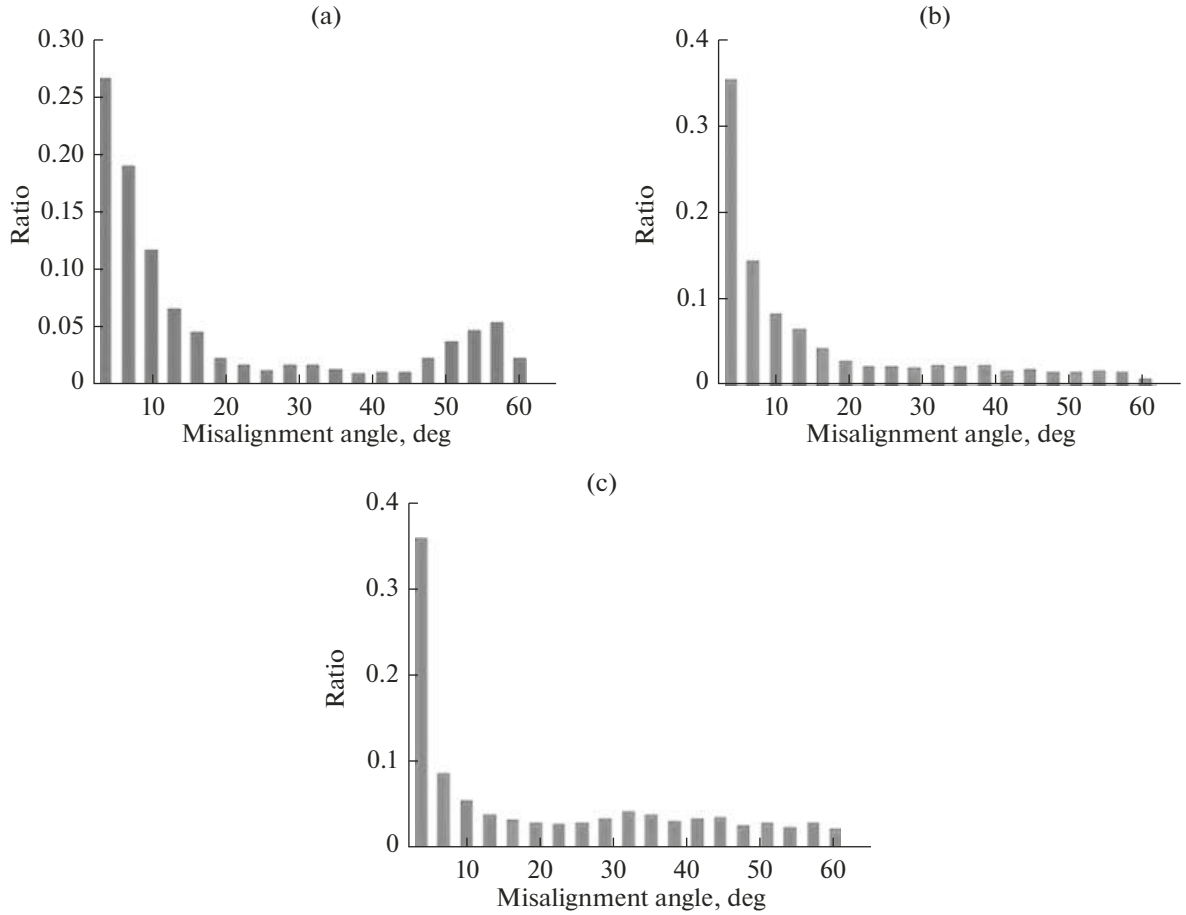

Fig. 5. Histograms of the misalignment angles plotted for grains of the samples after longitudinal fracture strength tests: (a) recrystallized state (σ = 113 MPa, ε = 12%, τ = 19600 s), (b) ultrafine-grained state (fast loading, σ = 113 MPa, ε = 9.4%, τ = 19600 s), (c) ultrafine-grained state (σ = 113 MPa, ε = 20%, τ = 36120 s).

We observed the contrast for dislocations in both (recrystallized and ultrafine-grained) samples studied when the active reflection vector was taken for the ⟨100⟩ family. In the recrystallized sample, the dislocations were located primarily in the plane of the foil, and in the ultrafine-grained sample, the dislocations were located perpendicular to it. The change in the dominant orientation of dislocations was associated, as shown earlier, with the difference in crystallographic texture of samples in the recrystallized and ultrafine-grained states.

Formation of possible dislocations was analyzed for the digital twin of the FCC aluminum lattice model using the Ovito software package [13] involving the dislocation analysis module [14]. There were screw dislocations 1/2[011] or 1/2[110] found in recrystallized and ultrafine-grained aluminum for a diffraction vector **g** = [200]. They are typical for FCC metals (aluminum, nickel, etc.), where sliding occurs in the system of planes ⟨110⟩. This corresponds to the basic sliding system ⟨110⟩ {111} in FCC metals. The Burgers vector 1/2⟨110⟩ corresponds to the smallest of all possible vectors in FCC metals for complete dislocation [15].

The analysis of grain size distribution after creep tests showed a decrease in grain length in both the recrystallized and UFG aluminum samples. The grain shape coefficient (GSC), which is the ratio of grain length to width, for the recrystallized state before and after testing was 2.3 ± 0.8 and 2 ± 1, respectively. The GSC for the ultrafine-grained state of the alloy before and after fast and prolonged loading was 4 ± 2, 3 ± 1, and 2 ± 1, respectively. A significant change in the GSC value for the creep tests at the UFG state suggested that the grains were broken during deformation, while in the recrystallized state, the alloy structure was crushed with a minor effect on the GSC.

The release of particles of secondary phases was detected when the distribution of elemental composition was investigated in the aluminum sample after the creep tests. The particles had higher concentration of silicon, carbon, and oxygen in the volume relative to the average. This was particularly evident in locations where the destruction process was localized. Accord-

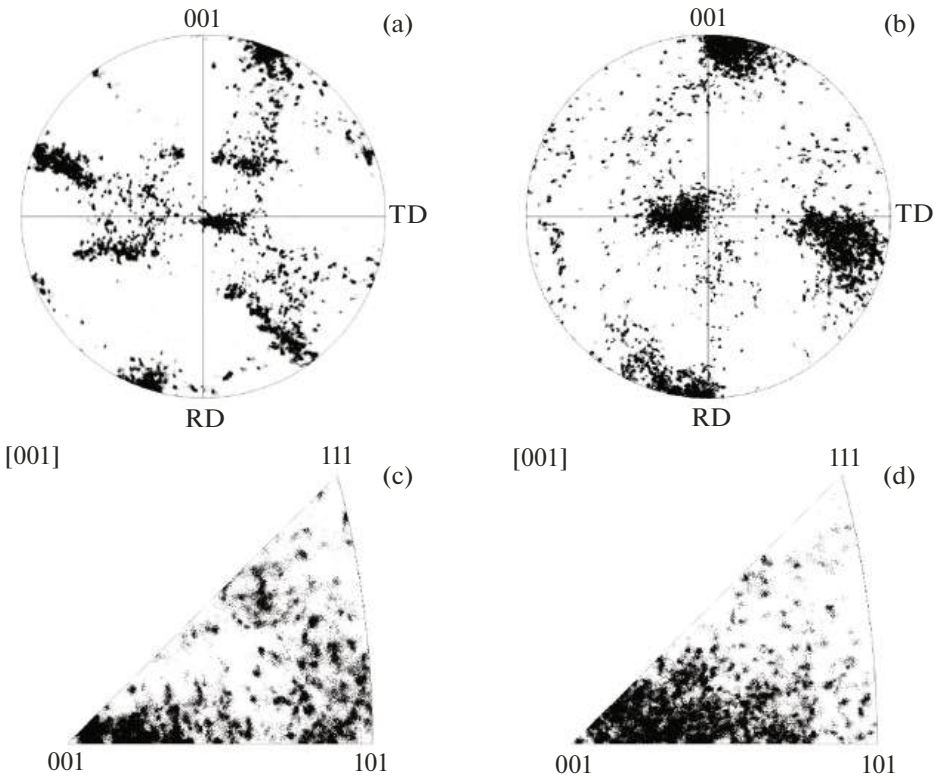

Fig. 6. Pole figures obtained for samples in the initial state (made from the area of the working base of the sample) in cross section: (a, c) recrystallized state, (b, d) ultrafine-grained state. (a, b) Direct and (c, d) reverse pole figures. The direction [001] is looking away and is perpendicular to the plane of the figure.

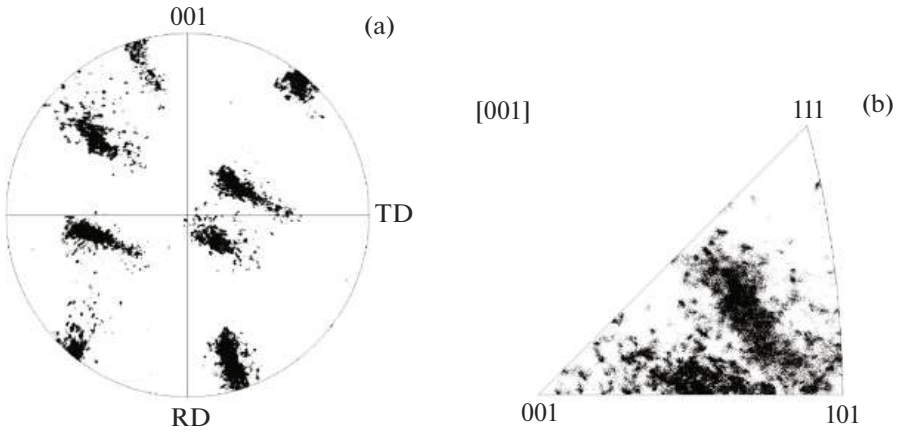

Fig. 7. Pole figures of recrystallized sample after long-term strength tests in the fracture region in the longitudinal section (σ = 113 MPa, τ = 19600 s). Direct (a) and reverse (b) pole figures. The direction [001] is looking away and is perpendicular to the plane of the figure.

ing to the model phase diagrams plotted using the CALPHAD (CALculation of PHAse Diagrams) method [16] in the Thermo-Calc software package [17], generation of particles of secondary phases requires a marked local increase in copper concentration, which is commonly observed at the grain boundaries, in triple junctions, and in defects having profound deformation. This feature was previously reported [18] in experiments featuring the release of copper-enriched particles of the secondary phase

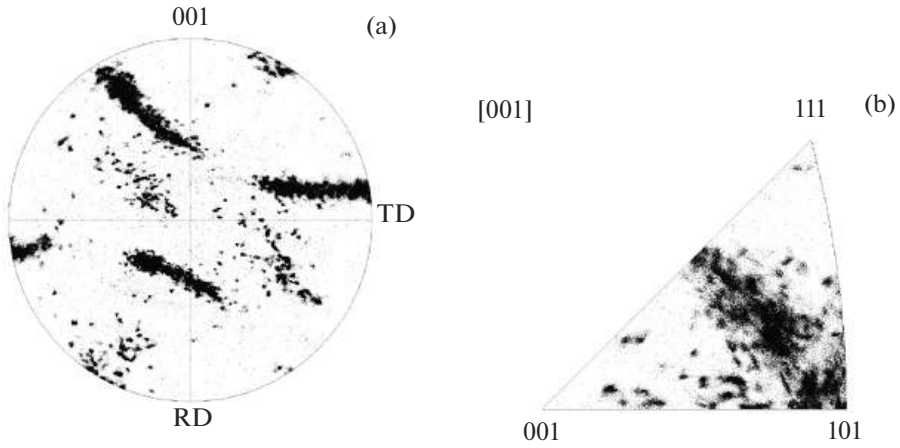

Fig. 8. Pole figures of ultrafine-grained sample after long-term strength tests in the fracture region in the longitudinal section (σ = 113 MPa, ε = 20%, τ = 36 120 s). Direct (a) and reverse (b) pole figures. The direction [001] is looking away and is perpendicular to the plane of the figure.

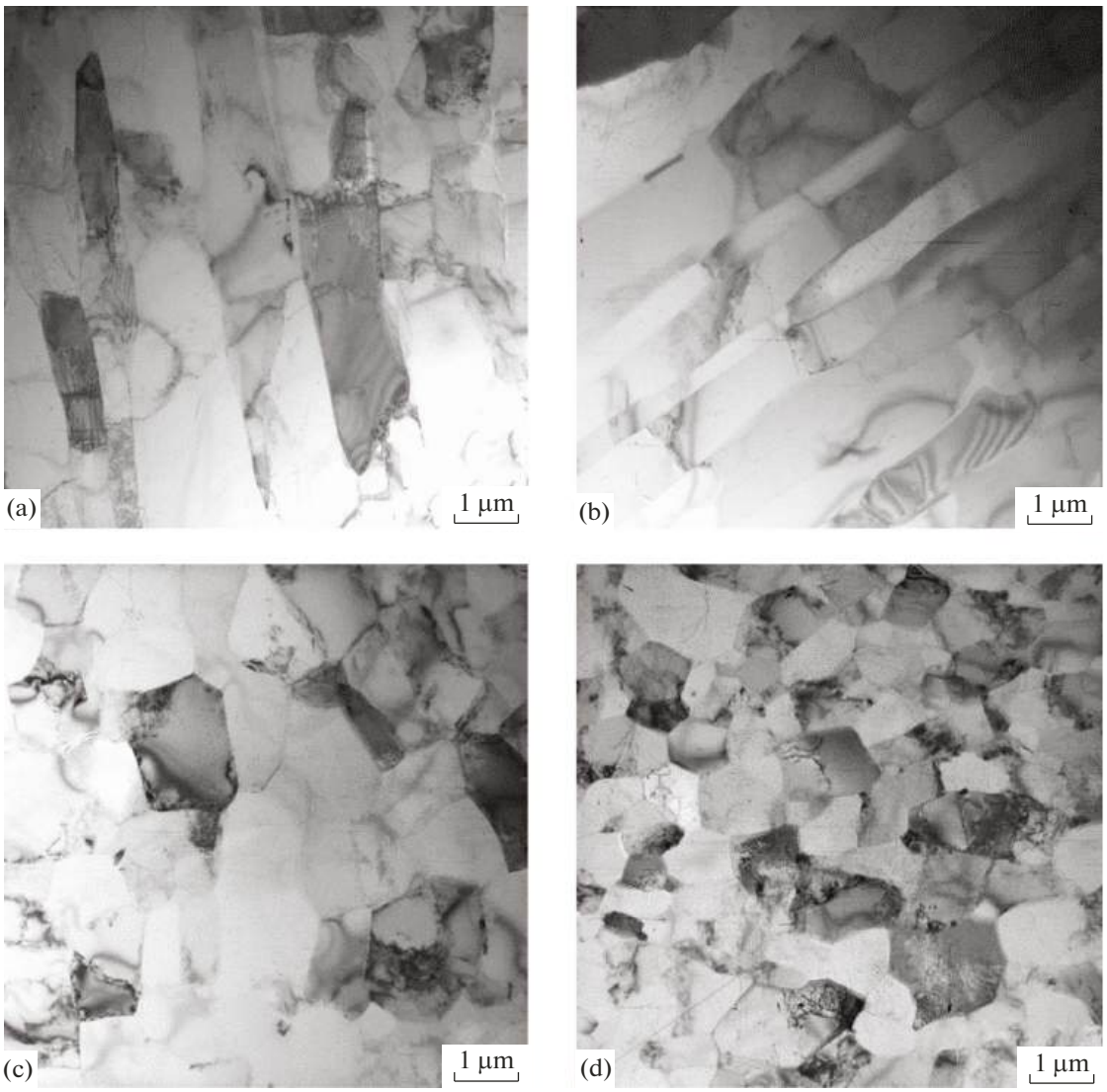

Fig. 9. TEM images of microstructure of aluminum alloy in the initial state: (a) recrystallized state, longitudinal section; (b) ultrafine-grained state, longitudinal section; (c) recrystallized state, cross section; (d) ultrafine-grained state, cross section.

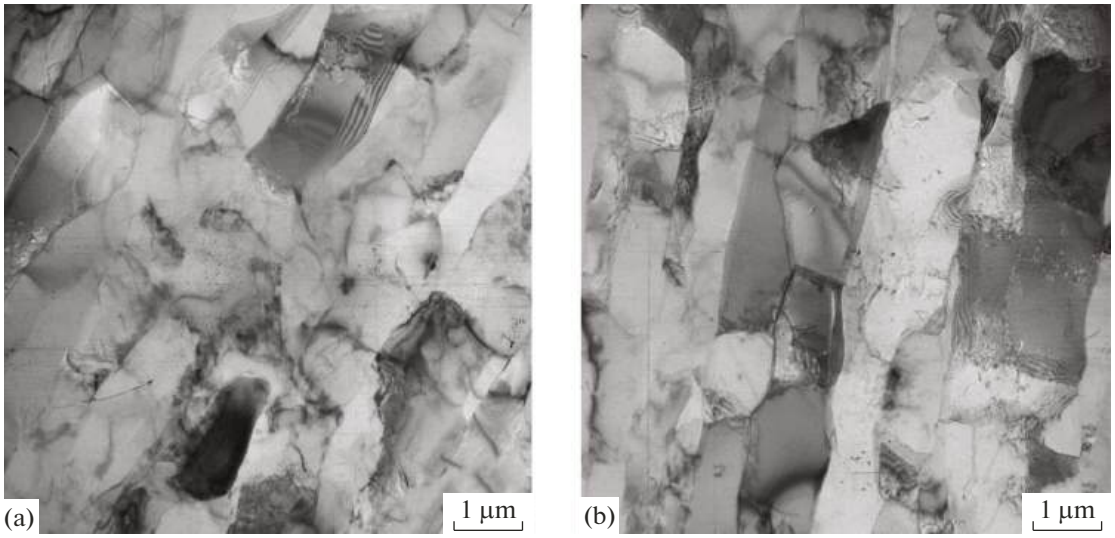

Fig. 10. TEM images of microstructure of aluminum alloy after creep tests: (a) recrystallized state, longitudinal section (σ = 113 MPa, ε = 12%, τ = 19600 s); (b) ultrafine-grained state, longitudinal section (σ = 113 MPa, ε = 20%, τ = 36120 s).

observed in the area where the aluminum alloy was destroyed. A model phase diagram was developed (Fig. 11) and it allowed identifying the phase as tetragonal type Al_2Cu-C16.

Energy-dispersive X-ray spectroscopy (EDX) was carried out in various local areas of thin aluminum foil, revealing the formation of individual large (about 150 nm) silicon-based particles at the grain boundaries.

In addition, aluminum carbide particles ranging in size from hundreds of nanometers to a micron were found in the structure of the alloy (Fig. 13).

The analysis of the designed phase diagram showing the chemical composition of a particle (Fig. 13b) led to the conclusion that the main volume fraction (80%) of these particles belongs to the Al_4C_3 aluminum carbide and to the B2 phase Al-(Cu,Fe).

These are the areas of plastic deformation where the release of particles of secondary phases was stimulated under conditions of creep. It can be assumed that the presence of these particles facilitated the development of the process of destruction.

CONCLUSIONS

The following conclusions were made in studying the microstructure and crystallographic texture of industrial aluminum alloy AD1 samples delivered in recrystallized and ultrafine-grained form after undergoing long- and short-term creep tests at $T \sim 0.3T_{melt}$ (100°C):

The large grains elongated along the axis of the original bar were crushed into smaller grains in the recrystallized structure during the process of creep. The average length decreased and the share of small-

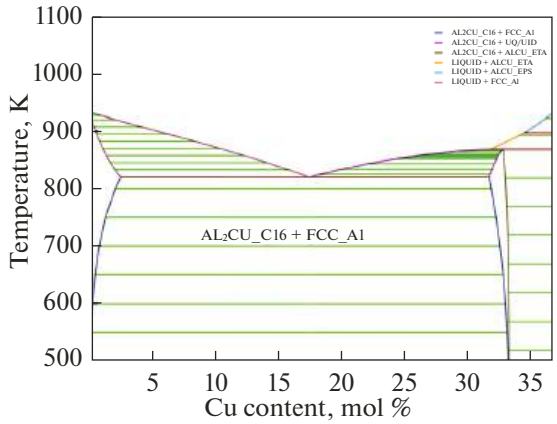

Fig. 11. Calculated phase diagram of Al–Cu system.

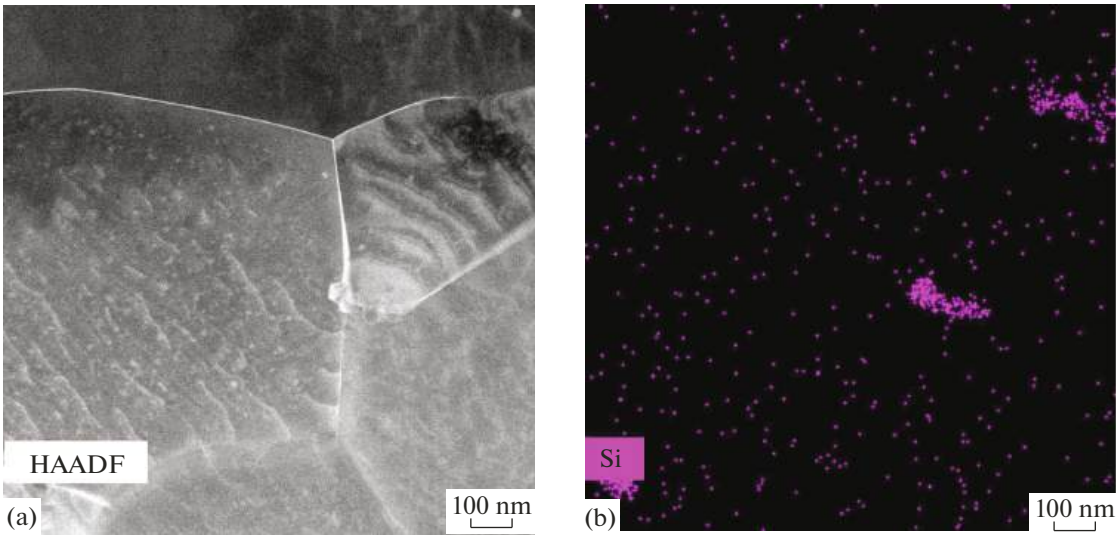

Fig. 12. TEM image (a) and EDX-analysis (b) of silicon-based particles in aluminum alloy structure.

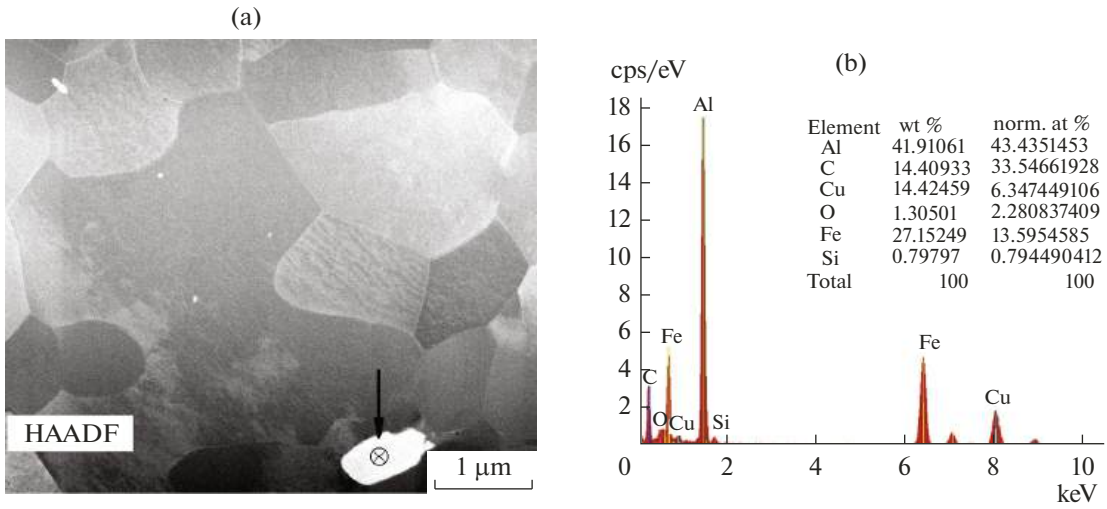

Fig. 13. SEM image (a) of a large particle in the structure of aluminum alloy after creep and its EDX analysis (b).

angle boundaries increased. In the ultrafine-grained structure, the average grain size increased, both in the longitudinal and in the transverse direction.

Strong radial texture having a texture axis [001] pointing along the bar axis in both types of samples was found. The sample in the recrystallized state featured an additional texture along the axis [011]. This texture was bimodal.

Following the creep tests, the texture axis changed from [001] to [011] in the ultrafine-grained samples. Long-term (10 h) creep tests resulted in a minor residual texture along the axis [001] in addition to the texture having the axis [011].

Particles of secondary phases—aluminum carbide, B2 phase (~1 μm in size), and silicon-based particles (~150 nm)—were found in the alloy structure. The complete elemental composition of silicon-based particles could not be established, and it was possible to assume the presence of oxide, carbide, or other compounds consisting of silicon and gas atoms. Since the particles detected are rarely found in the volume of the aluminum matrix, they are likely to have little effect on the progress of the creep process. The application of the method of construction of calculated phase diagrams to analyze release of particles during long-term strength tests allowed interpreting the experimental data in better detail.

FUNDING

In the part dealing with the study of the structure, the work was carried under financial support of the Russian Foundation for Basic Research (project no. 19-58-26005). The part of studies dealing with analyzing the features of applying computer modeling to explore the nature of generated secondary phases under different processing of multicomponent alloys was funded by the Russian Science Foundation (project no. 22-13-00324). The study of the phase composition was carried out under state assignment FFSG-2024-0016, no. 124020500064-2.

Structural studies were carried out using the scientific equipment at the Common Use Center of the Federal Scientific Research Center Crystallography and Photonics, Russian Academy of Sciences (Moscow).

CONFLICT OF INTEREST

The authors of this work declare that they have no conflicts of interest.

REFERENCES

1. Betekhtin, V.I. and Kadomtsev, A.G., Evolution of microscopic cracks and pores in solids under loading, *Phys. Solid State,* 2005, vol. 47, no. 5, pp. 825–831. https://doi.org/10.1134/1.1924839
2. Rabotnov, Yu.N., *Polzuchest' elementov konstruktsii* (Creep of Construction Elements), Moscow: Nauka, 1996.
3. Kachanov, L.M., *Osnovy mekhaniki razrusheniya* (Fundamentals of Fracture Mechanics), Moscow: Nauka, 1974.
4. Betekhtin, V.I., Kadomtsev, A.G., and Narykova, M.V., Evolution of a defect structure duringcreep tests of ultrafine-grained metals and alloys produced by severe plastic deformation, *Phys. Solid State,* 2020, vol. 62, no. 2, pp. 318–324. https://doi.org/0.1134/S1063783420020067
5. Cheremskoi, P.G., Slezov, V.V., and Betekhtin, V.I., *Pory v tverdom tele* (Pores in Solid), Moscow: Energoatomizdat, 1990.
6. Kolobov, Yu.R., Nanotechnologies for the formation of medical implants based on titanium alloys with bioactive coatings, *Nanotechnol. Russ.,* 2009, vol. 4, pp. 758–775. https://doi.org/10.1134/S1995078009110020
7. Rybin, V.V., *Bol'shie plasticheskie deformatsii i razrushenie metallov* (Large Plastic Deformations and Destruction of Metals), Moscow: Metallurgiya, 1986.
8. Kolobov, Yu.R., Regularities and mechanisms of formation of submicro-, nano-, and ultrafine-grained structures and mechanical properties of metals and alloys under different treatments, *Russ. Phys. J.,* 2018, vol. 61, no. 4, pp. 611–623. https://doi.org/10.1007/s11182-018-1440-4
9. Noskova, N.I. and Mulyukov, R.R., *Submikrokristallicheskie i nanokristallicheskie metally i splavy* (Submicrocrystalline and Nanocrystalline Metals and Alloys), Yekaterinburg: Ural Branch Russ. Acad. Sci., 2003.
10. Kozlov, E.V., Glezer, A.M., Koneva, N.A., Popova, N.A., and Kurzina, I.A., *Osnovy plasticheskoi deformatsii nanostrukturnykh materialov* (Fundamentals of Plastic Deformation of Nanostructured Materials), Moscow: Fizmatlit, 2016.
11. *Proc. 16th Sagamore Army Materials Research Conf. "Ultrafine-Grain Metals" (Raquette Lake, New York, August 19–22, 1969),* Burke, J.J., Reed, N.L., and Weiss, V., Eds., New York: Syracuse Univ. Press, 1970.
12. Montoya, E., Bals, S., Rossell, M.D., Schryvers, D., and Van Tendeloo, G., Evaluation of top, angle, and side cleaned FIB samples for TEM analysis, *Microsc. Res. Tech.,* 2007, vol. 70, no. 12, pp. 1060–1071. https://doi.org/10.1002/jemt.20514
13. Stukowski, A., Visualization and analysis of atomistic simulation data with OVITO—the Open Visualization Tool, *Modell. Simul. Mater. Sci. Eng.,* 2009, vol. 18, no. 1, p. 015012. https://doi.org/10.1088/0965-0393/18/1/015012
14. Stukowski, A., Bulatov, V.V., and Arsenlis, A., Automated identification and indexing of dislocations in crystal interfaces, *Modell. Simul. Mater. Sci. Eng.*, 2012, vol. 20, no. 8, p. 085007. https://doi.org/10.1088/0965-0393/20/8/085007
15. Grigorovich, V.K. and Sheftel', E.N., *Dispersionnoe uprochnenie tugoplavkikh metallov* (Dispersion Hardening of Refractory Metals), Moscow: Nauka, 1988.
16. Kaufman, L. and Bernstein, H., *Computer Calculation of Phase Diagrams*, New York: Academic, 1970.
17. Andersson, J.O., Helander, T., Höglund, L., Shi, P., and Sundman, B., Thermo-Calc & DICTRA, computational tools for materials science, *Calphad,* 2002, vol. 26, no. 2, pp. 273–312. https://doi.org/10.1016/S0364-5916(02)00037-8
18. Manohin, S.S., Betekhtin, V.I., Kadomtsev, A.G., Narykova, M.V., Amosova, O.V., Kolobov, Yu.R., and Lazarev, D.V., Study of the structural features of microcrystalline aluminum after tests for long-term strength, *Phys. Solid State,* 2023, vol. 65, no. 1, p. 126. https://doi.org/10.21883/PSS.2023.01.54986.492

Translated by V. Vetrov